Engineering Geology 175 (2014) 58–73

Contents lists available at ScienceDirect

Engineering Geology

journal homepage: www.elsevier.com/locate/enggeo

Characteristics of earthquake- and rain-induced landslides near the epicenter of Wenchuan earthquake

S. Zhang [a], L.M. Zhang [a,*], T. Glade [b]

[a] Department of Civil and Environmental Engineering, The Hong Kong University of Science and Technology, Clear Water Bay, Hong Kong
[b] Department of Geography and Regional Research, University of Vienna, Universitaetsstr. 7, 1010 Vienna, Austria

ARTICLE INFO

Article history:
Received 17 September 2013
Received in revised form 15 March 2014
Accepted 19 March 2014
Available online 2 April 2014

Keywords:
Landslides
Rain-induced landslides
Debris flows
Slope stability
Risk analysis
Wenchuan earthquake

ABSTRACT

Numerous landslides were triggered by the 12 May 2008 Wenchuan earthquake in China, particularly near the epicenter. During the rainy season in 2010 after the earthquake, much of the landslide debris was reactivated, causing a large number of fatalities. The earthquake has a significant impact on the subsequent rain-induced landslides. Based on interpretation of satellite images taken in 2008 and 2010, combined with yearly field investigations, this paper attempts to (1) map the earthquake-induced landslides near the epicenter; (2) present the distribution of the landslides occurring during a subsequent extreme storm in the same area; and (3) compare the distribution characteristics of the earthquake-induced landslides and the rain-induced landslides. Through this study, the following findings were obtained: (1) the internal relief of the landslides in the study area is much higher than that in other affected regions of the Wenchuan earthquake zone; (2) the landslide area in hard rocks (i.e. the granite and diorite zones) is much larger than that in alluvium; (3) the volume of hill-slope loose deposits decreased while the volume of channel deposits increased during the process of mass transportation caused by rainfall after the earthquake; (4) during the rainy seasons after the earthquake, the density of landslides increased while the area of landslides decreased significantly and the type of landslides transformed from debris slides to debris flows; and (5) the rain-induced landslides are less steeper than the earthquake-induced landslides.

1. Introduction

A landslide is defined as a downward and outward movement of slope-forming materials composed of natural rocks, soils, artificial fills or combinations of these materials (Varnes, 1958). It includes several typical failure processes such as slides, falls, and flows. Landslide may have a direct effect upon human life and result in economic costs (Glade et al., 2005). Rainfall and earthquakes are two common triggering mechanisms of landslides (e.g. Keefer, 1984). Much has been learned about the identification and description of earthquake-induced landslides from previous high-magnitude earthquakes that occurred in mountainous regions (Keefer, 1984; Jibson and Keefer, 1989; Harp and Jibson, 1996; Jibson et al., 2004; Khazai and Sitar, 2004; Lin et al., 2006; Sato et al., 2007; Qi et al., 2010; Gorum et al., 2011; Tang et al., 2011; Xu et al., 2011). Among these, Keefer (1984) studied the relationship between the distribution of earthquake-induced landslides and seismic parameters based on data from 40 historical earthquakes. The study showed that the area affected by landslides in an earthquake correlates with the earthquake magnitude. Certain threshold levels of ground shaking are necessary to trigger various types of landslides. Hasi et al. (2010) believed that the distribution of landslides induced by the Iwate–Miyagi Inland earthquake was primarily controlled by the fault rupture, which showed a very distinct "hanging wall" effect. Unlike landslide distributions in most previous earthquakes, Jibson et al. (2004) found that the landslides triggered by the 2002 Denali fault earthquake, Alaska, were mainly concentrated in a narrow zone 30-km in width that straddled the fault rupture over its entire 300 km length.

The long-term impact of an earthquake on the slope stability during the wet season is significant (e.g. Lin et al., 2006). Attention must be paid to investigating detailed characteristics of rain-induced landslides after the earthquake. However, less research has been done on this topic. By comparing the occurrence of landslides in the Choushui River watershed through eight SPOT images that covered the period from 1996 to 2001, the influence of the Chi-Chi earthquake on the subsequent rainfall-triggered landslides was investigated by Lin et al. (2006). The density of rain-induced landslides increased substantially after the earthquake and the landslide locations changed as well.

The 12 May 2008 Wenchuan earthquake in China triggered more than 15,000 landslides in the form of slides and rock falls, which resulted in approximately 20,000 fatalities (Yin, 2008; Yin et al., 2009). During the wet season, the debris of these landslides may lose stability due to

* Corresponding author.
E-mail addresses: zhangshuaiqj@ust.hk (S. Zhang), cezhangl@ust.hk (L.M. Zhang), thomas.glade@univie.ac.at (T. Glade).

http://dx.doi.org/10.1016/j.enggeo.2014.03.012
0013-7952/

rainfall infiltration, and can easily evolve into deadly debris flows. The 45 km reach of Province Road 303 (PR303) is the only path from the epicenter of the Wenchuan earthquake, Yingxiu, to the Research and Conservation Centre for Giant Panda at Wolong (Figure 1). Numerous landslides were triggered on both sides of the road during the earthquake. The reconstruction of PR303 started in April 2009. Although effort has been made to remove or strengthen some unsafe slopes, many deposits at high elevations are unstable or have not been identified. During the rainy season in 2010, widespread landslides were induced by a storm, which caused a large number of fatalities and serious damage to the reconstructed road (Zhang et al., 2012, 2013). It is expected that rain-induced slope failures will continue to occur in the future. Therefore, it is important to understand the impact of the Wenchuan earthquake on the occurrence of subsequent rain-induced landslides. This paper attempts to (1) map the earthquake-induced landslides along PR303 near the epicenter; (2) present the distribution of the landslides that occurred during an extreme storm event in the same area; (3) compare the distribution characteristics of the earthquake-induced landslides and the rain-induced landslides. In this study, earthquake-induced debris slides and rock falls, and rain-induced debris slides and debris flows, in the landslide terminology of Cruden and Varnes (1996), are all included.

2. Study area

2.1. Geological settings

Province Road 303 is primarily along the Yuzixi River that is bounded by terrains with elevations from 880 m at Yingxiu Town to 5040 m at the highest mountain peak. The terrain is rugged with steep slopes exceeding 40° in many places. A digital elevation model (DEM) was adopted to study the topography in the study area. The DEM was derived from digitized contours with 20 m elevation intervals mapped by Sichuan Highway Department (2011) in December 2008. Results of a slope gradient analysis in the geographic information system (GIS) are shown in Fig. 2. From milestone K1 to K45, the slope angles mainly range between 20° and 70° on both sides of the highway.

The highway goes across four faults and is partly located on the hanging wall of the Yingxiu–Beichuan fault where strong ground motions were up to a peak horizontal ground acceleration of 0.96 g during the Wenchuan earthquake (Li et al., 2008). The geological setting between Yingxiu and Gengda from K1 to K18 mainly consists of medium fine-grained granite, diorite and alluvium (Figure 3). The hard rocks explain why the topography of the study area can be so steep (Figure 2). Between Gengda and Wolong from K18 to K45, the lithology turns into phyllite, sandstone and limestone starting from the Maoxian–Wenchuan fault (Figure 3). Such a special lithological contrast contributed to the contrasting landsliding scenarios taking K18 (near Gengda) as a boundary. Strong weathered rock slopes with outward inclined joint sets were widely distributed on both sides of the highway from K1 to K45, especially on the upper part of the gullies. In this paper, an area of 85 km^2 between Yingxiu and Gengda shown in Fig. 3 is investigated in detail.

2.2. Precipitation conditions

Based on rainfall records from 1957 to 1981 at 5 rainfall monitoring stations distributed near the study area, an annual rainfall distribution map was developed using Kringing in ArcGIS (Figure 4). The annual rainfall amount varies greatly due to the variations in topography along the highway. The average monthly rainfall ranges from 9.2 mm in December to 278.4 mm in August (Table 1), approximately 66–76% of the rainfall occurs during the rainy season from June to August. The average number of rainy days is 202.7 during the observing years. After the Wenchuan earthquake, the study area suffered from several storms. Of these, the storm on 14 August 2010 was the heaviest, with a precipitation of 163 mm in 8 h. The hourly rainfall records from a precipitation station in Yingxiu Town were used to analyze the triggering of rain-induced landslides.

3. Investigation methodology

Digital photo interpretation techniques and field verifications were combined to characterize the landslides in the study area. Important aspects in the recognition of landslides are the size of landslide features, the difference in spectral characteristics between the landslides and their surrounding areas, and the morphological expression (Mantovani et al., 1996). Features such as scarps, disrupted vegetation

Fig. 1. Location of the study area, the study area is marked.

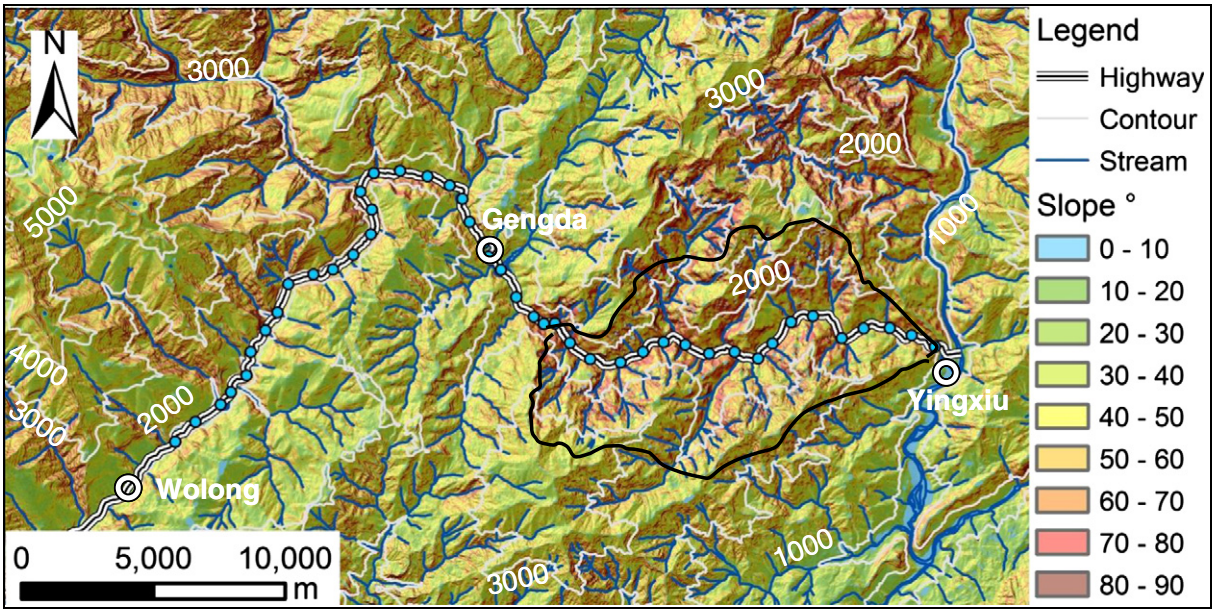

Fig. 2. Slope angle in the study area.

cover, and state of landslide deposits are used in conjunction with morphological features. Quickbird images taken on 30 May 2008 (shortly after the Wenchuan earthquake) and Worldwide-2 images taken on 18 December 2010 (shortly after an extreme storm) were prepared to identify the landslides in the study area. The resolutions of the Quickbird images and Worldwide-2 images were 0.61 m and 2.5 m, respectively. The smallest landslide area that can be interpreted reasonably accurately from the satellite images was 367 m^2. From 2008 to 2010, yearly field investigations were conducted to check the hazardous areas, the source material conditions, the depositional fans and the

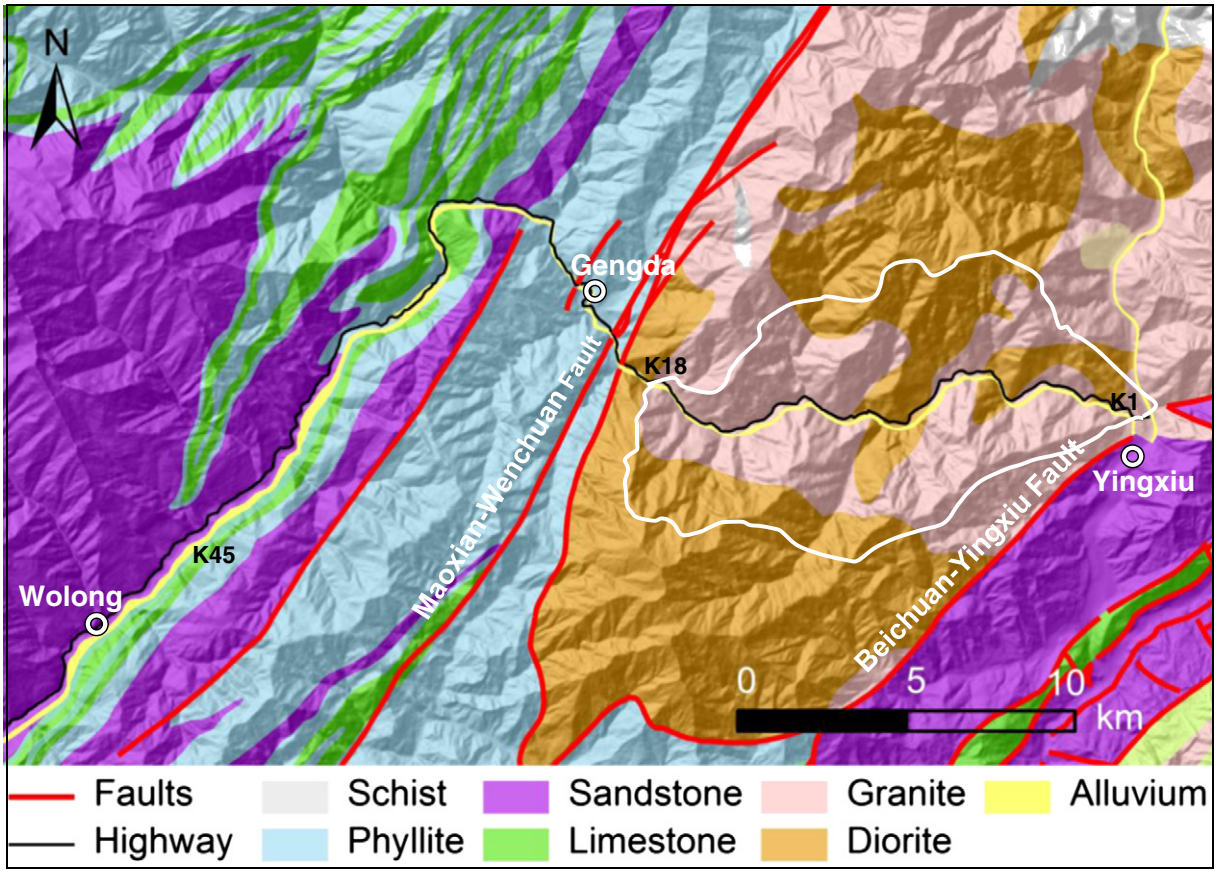

Fig. 3. Geological conditions and tectonic structures in the study area.

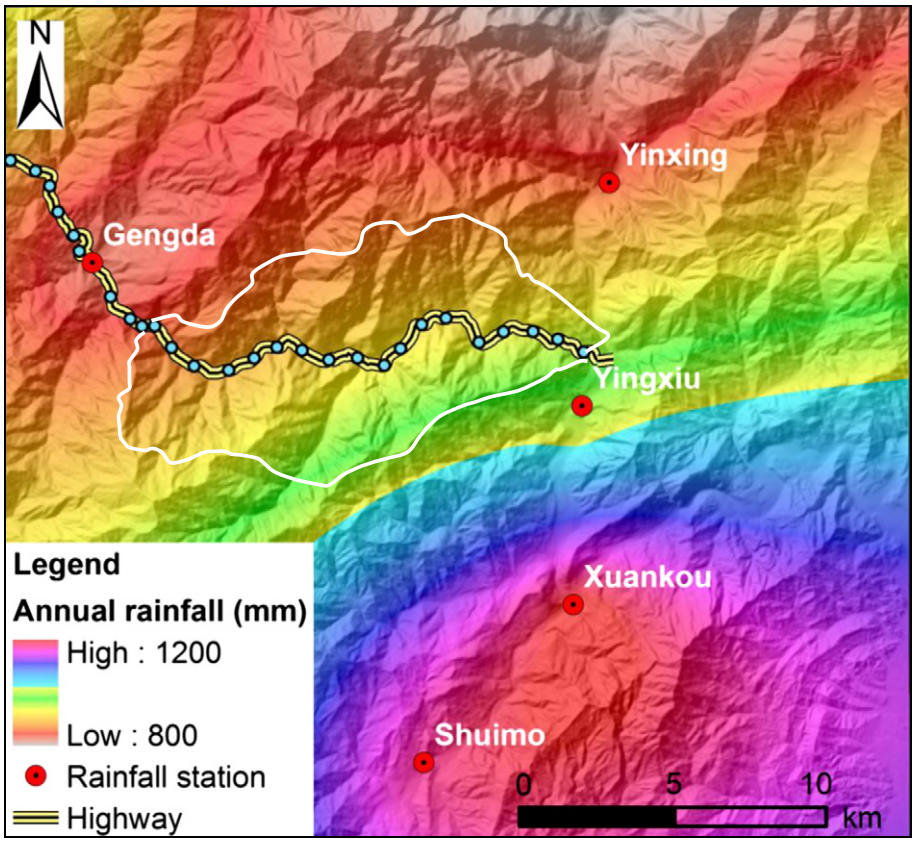

Fig. 4. Annual average rainfall across the study area based on 25 years of climatology records (1957–1981) from 5 rain gauges at Yinxing, Yingxiu, Gengda, Xuankou, and Shuimo.

depths of run-out materials. ArcGIS was used to digitize the landslides and estimate the landslide area. The DEM created after the earthquake was adopted to calculate the slope angles of the landslide deposits by averaging the slopes of all pixels that fell within a given landslide.

The volumes of the hill-slope deposits, channel deposits, and run-out debris flow materials were estimated by multiplying the respective covering area by the average thickness of the deposits according to Martin et al. (2002). By measuring the scar and deposition areas of 25 selected hill-slope deposits (Figure 5), the average ratio of the scar area and the deposition area was determined as 1:3. The deposit thicknesses in the scar area and the deposition area, measured using a laser range finder in-situ, are on average 1 m and 3 m, respectively. The thicknesses of the channel deposits were measured at exposed locations along the gully, which were on average 10 m. The thickness of the run-out debris was determined by borehole drilling at the middle part of debris fan, trenching in the frontal area and direct measurement at exposed locations around the debris fan (Figure 5). The deposition areas of the debris flows and the covering areas of the hill-slope deposits were calculated on ArcGIS based on the satellite images (Figure 5). Therefore, based on the covering area, the volume of each loose soil deposit and the total volume of the run-out debris materials can be evaluated.

4. Landslide inventory along the highway

4.1. Earthquake-induced landslides on 12 May 2008

On 12 May 2008, the Wenchuan earthquake produced widespread shallow landslides along PR303. Most of them were concentrated on the hanging wall of the Yingxiu–Beichuan fault due to the "hanging wall" effect (Lin et al., 2000; Hasi et al., 2010; Xu et al., 2011). Therefore, a total area of 85 km^2 near the epicenter along PR303 from Yingxiu to Gengda (K1 to K18) was selected for this study. As shown in Figs. 6 and 7, the road was largely buried or severely destroyed by densely populated loose landslide deposits. A total of 305 shallow slides were identified and are shown in Fig. 8. The slope gradients of these 305 loose deposits range from 6° to 54°. The steepest loose deposit is No. 206 with an average gradient of 54° located within the Luobaoshu Ravine. The largest one is No. 113 in the Dayingou Ravine with a slope gradient of 21° and a covering area of 0.46 km^2, located at elevations between 2300 m and 3190 m. A total of 28 channel deposits were identified, which are distributed in various catchments (Figure 8). The largest one has a covering area of 0.72 km^2 and a volume of 1.05×10^6 m^3, which is located within the catchment near K10. The total volume of all the loose deposits between K1 and K18 is estimated to be 66.69×10^6 m^3 (Table 2).

Table 1
Monthly precipitation in Yingxiu.

Month	l	2	3	4	5	6	7	8	9	10	11	12
Rainfall (mm)[a]	10.3	19.5	51.3	86.1	107.7	131.2	277.5	278.4	170.1	80.9	31.3	9.2

[a] Based on rainfall data from 1957 to 1981.

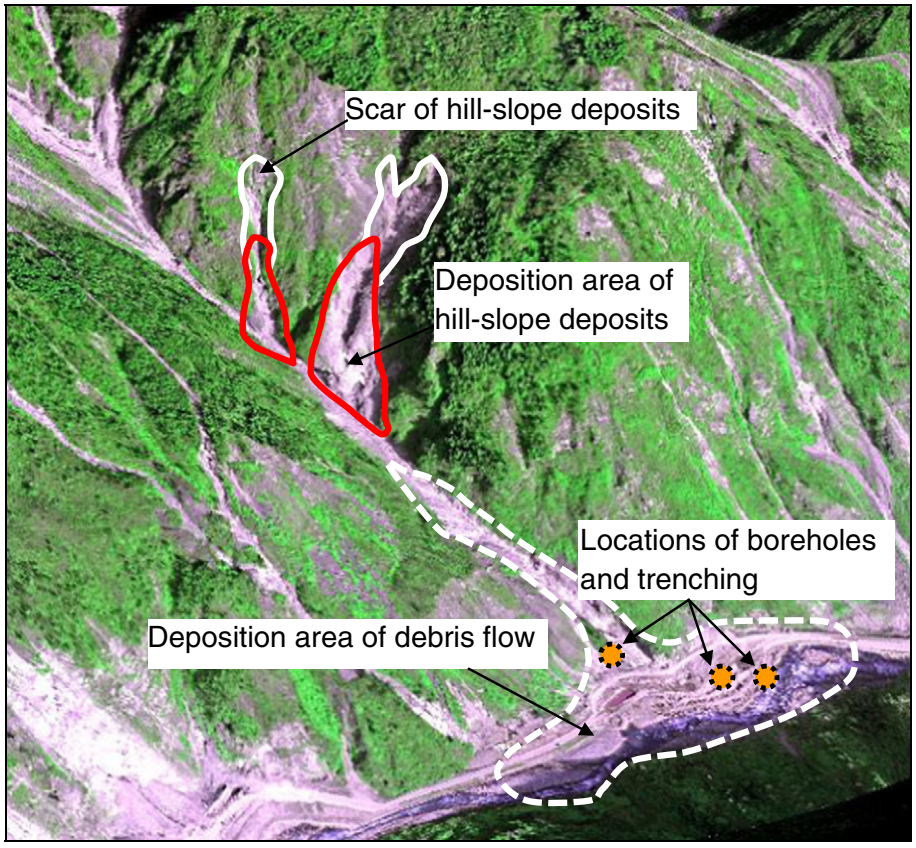

Fig. 5. Data measured on ArcGIS or during field investigations.

4.2. Rain-induced landslides during the 14 August 2010 storm

From 17:00 on 12 August 2010, a heavy rainstorm swept Yingxiu and its vicinity. The hourly and cumulative rainfall records are shown in Fig. 9. A cumulative rainfall of 226 mm was recorded within 39 h from 17:00 on 12 August to 7:00 on 14 August. Particularly, a cumulative rainfall amount of 185 mm was recorded by about 4:00 am on 14 August 2010, when local residents witnessed widespread landslides and debris flows in the study area (Figure 10).

A total of 351 fresh rain-induced landslides were identified in the study area (Figure 11). These fresh landslides included 322 reactivated shallow landslides which occurred on the pre-existing landslides induced in 2008, and 29 new landslides which occurred in locations not affected by the landslides in 2008. Among them, the largest reactivation landslide was No. 248 located at the lower part of the Luobaoshu Ravine with a covering area of 0.16 km^2 and a volume of 0.38×10^6 m^3 (Figure 11). Image analysis shows that the number of channel deposits increased to 35 after the rainfall event in 2010 as illustrated in Table 3. Due to the influence of cloud shadow in the satellite images taken in 2010 (Figure 10), the number of the rain-induced landslides might be underestimated.

During the storm in August 2010, 12 channelized debris flows and 14 hill-slope debris flows were also triggered along PR303 (Figure 12 and Table 4). Field investigations revealed that the channelized debris

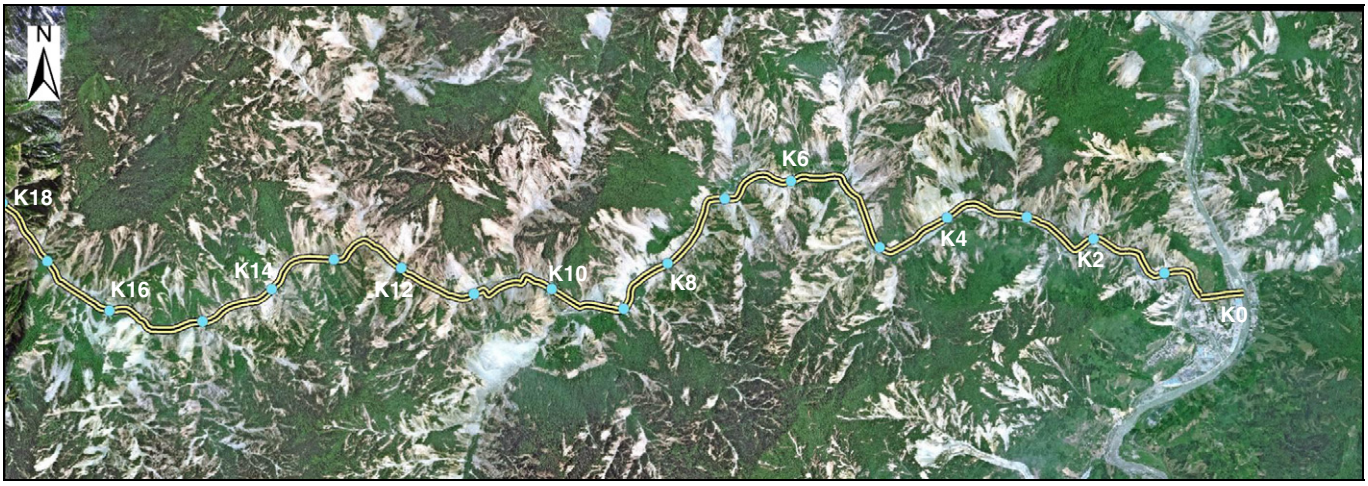

Fig. 6. Satellite image taken on 30 May 2008 showing numerous earthquake-induced landslides distributing along the highway.

Fig. 7. Damage to the highway during the earthquake: (a) overall view; (b) damaged road; and (c) fatal landslide.

flows were initiated in the form of channel-bed failure, while the hill-slope debris flows were mainly initiated by firehose effect and rilling (Chen et al., 2012, 2013). Torrents would form in a channel during a storm. Under the combination of gravity and the scour of the torrents, an increasing amount of bed materials could be entrained into the flow. When the medium-size particles were mobilized by the turbulent flow in a large scale, the channel-bed failure would be initiated. The firehose effect is a phenomenon that the solid materials are mobilized by concentration of water flow just like being washed away by a firehose (Chang et al., 2011; Chen et al., 2012). Rilling is generally attributed to the concentration of overland flow in micro-channels (Godt and Coe, 2007). In the study area, the runoff from upstream channels flew down and washed away the colluvium on bedrock; the firehose effect occurred mostly on steep bedrock slopes with thin layers of materials. Rills grew by erosion, deepening of plunge pools by turbulent flows and bank failures. Materials entrained by rills finally entered the channels. Rilling tended to occur on relatively gentle slopes with thick covering materials. The debris flow events resulted in the destruction of the reconstructed road (i.e., PR303) rebuilt after the Wenchuan earthquake (Figure 13b) and fatalities (Figure 13c). The runout debris blocked the Yuzixi River and formed landslide lakes (Figure 13d), raising the riverbed by at least 13 m compared with that before the debris flows. The total deposition area of the debris flows was 2.68 km^2, of which 2.33 km^2 was due to channelized debris flows and 0.35 km^2 due to hill-slope debris flows (Table 3). The most severe one was a channelized debris flow in the Xiaojiagou Ravine, No. CD06, which had a runout material volume of 1.17×10^6 m^3 and a runout distance of 593 m (Table 4).

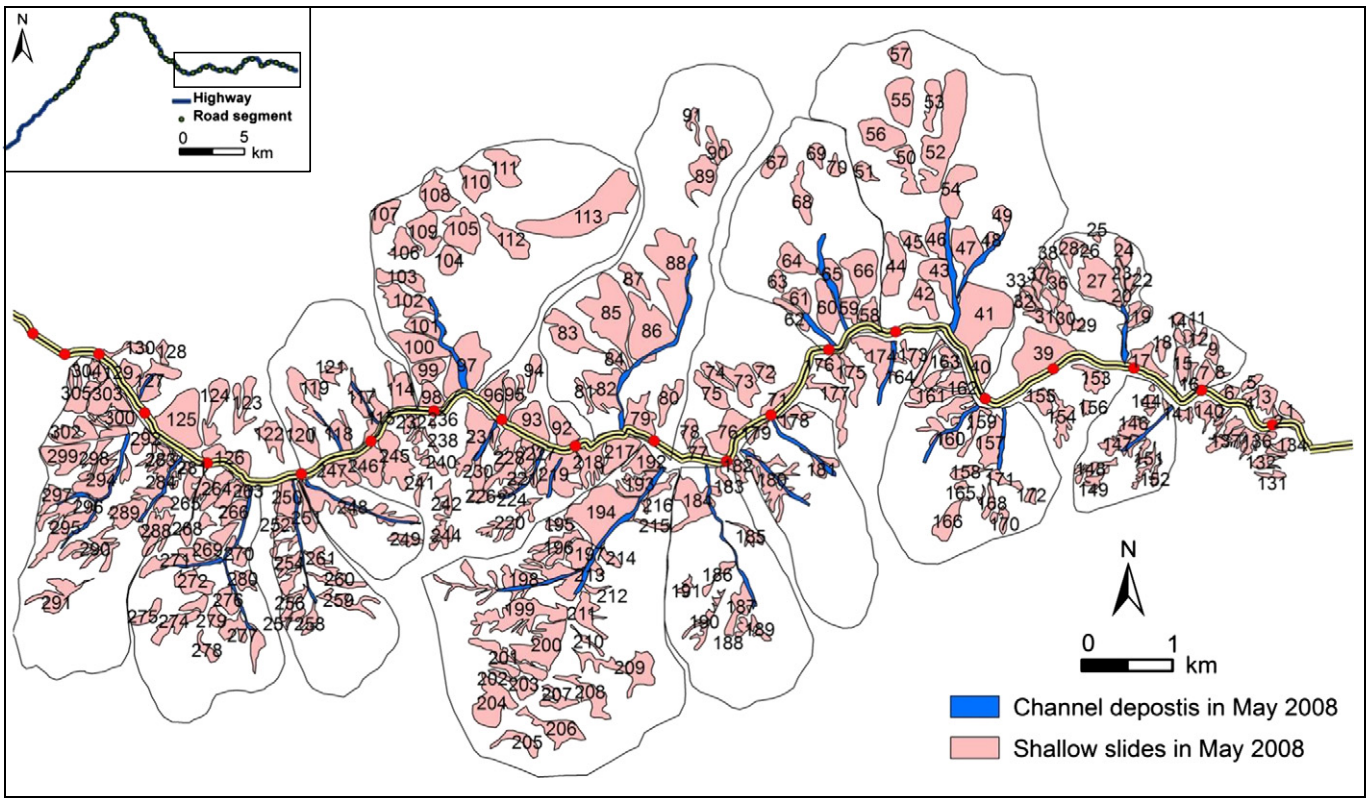

Fig. 8. Inventory of the earthquake-induced landslides within the study area.

5. Redistributions of landslides induced by rainfall

5.1. Evolution of source materials

In the study area, the distributions of the volume of landslides along the highway shortly after the earthquake in 2008 and after the rainstorm in 2010 are shown in Fig. 14. The box plots display the full range of variations of landslide volume (from the minimum to the maximum) in every 2 km along the road. The total volume of the 305 hill-slope deposits shortly after the Wenchuan earthquake was 54.30 million m^3 and the total volume of the channel deposits was 12.39 million m^3 (Table 2). The August 2010 storm triggered 351 fresh landslides but the total volume of these landslides was significantly smaller than that triggered by the earthquake in 2008 (Figure 15). The volumes of the hill-slope deposits from the reactivation landslides, new landslides and original landslides were 15.42, 1.52 and 31.28 million m^3, respectively. However, the amount of channel deposits increased obviously after the storm in 2010, with a total volume of 16.94 million m^3 (Table 3).

Comparing the satellite images taken on 30 May 2008 and 18 December 2010 (Figures 6 and 10), the evolution of the loose materials can be quantified. The catastrophic Wenchuan earthquake not only triggered serious coseismic landslides but also disturbed the surface strata seriously along the highway. Colluvium materials were widely distributed on the hill slopes along PR303, which provided source materials for the subsequent debris flows (Figure 16b). A considerable portion of the hill-slope deposits had either slid or been washed into the channels by surface runoff during rainy days (Figure 16c). In the rainy season, the hill-slope deposits gradually evolved into channel deposits and the materials in the channels gradually moved toward the gully mouth (Figure 16d), which finally ran out as debris flows under storm conditions (Figure 16e). Thus the volume of the hill-slope loose deposits decreased while the volume of the channel deposits increased from 2008 to 2010. The reactivation of the hill-slope loose deposits was caused by rainfall infiltration and the decrease of the shear strength of soil (Zhang et al., 2004, 2011; Lin et al., 2006; Zhao et al., 2013; Zhao and Zhang, 2014). Furthermore, some substrata on the hill slopes became unstable due to the presence of numerous tension cracks induced by the strong ground motion. These factors intensified the landslide activities during the subsequent heavy rain events.

Table 2
Landslide materials identified based on Quickbird images taken on 30 May 2008.

Type	Number	Total area (km^2)	Volume (10^6 m^3)
Hill-slope deposit	305	24.02	54.30
Channel deposit	28	1.24	12.39
Total	–	25.26	66.69

5.2. Changes in area and number of landslides

The Wenchuan earthquake has greatly aggravated landslide activities in the study area. Image analysis shows that the area of earthquake-induced landslides in 2008 was 24.02 km^2 (Table 2). After the rainstorm in 2010, the area of all types of landslides was 20.67 km^2. The rain-induced fresh landslide area (including the areas of the reactivated and new landslides) was 7.26 km^2, which was only one third of the earthquake-induced landslide area (Table 3). However, the number of landslides after the 2010 storm event was identified as 590, which increased by 93.4% compared with the number of landslides in 2008.

What caused these unexpected changes in the area and density of the landslides over time? The hill-slope landslides induced by the Wenchuan earthquake could be categorized as debris slides based on the classification of landslides proposed by Cruden and Varnes (1996). It can be seen that there is a distinct scar zone that separates the sliding material from more stable underlying material (Figure 17a and c). Due to the heavy precipitation in August 2010 (Figure 9), the hill-slope loose material formed in 2008 reactivated and ran out. The debris slides

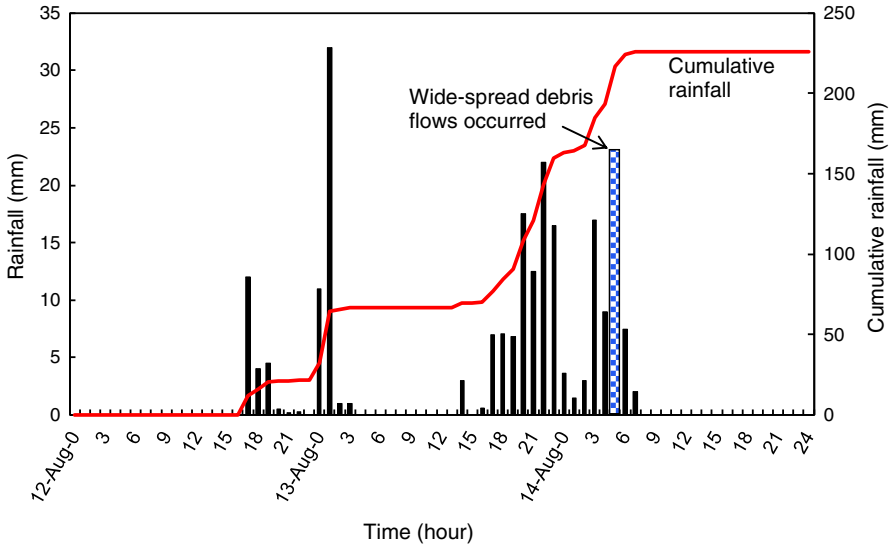

Fig. 9. Distributions of hourly and cumulative rainfall between 12 and 14 August 2010.

transformed into elongated debris flows with longer runout distances, forming a bowl at the front as shown in Fig. 17b (Cruden and Varnes, 1996). Two years after the earthquake, the vegetation gradually recovered, which alleviates the erosion of the loose material during the rainy season. The rainstorm caused a loose deposit to lose stability locally. Thus, a single original debris deposit could develop into several smaller debris flows as illustrated in Fig. 17. This explains why the landslide number increased while the landslide area decreased in 2010 (Tables 2 and 3).

5.3. Change in landslide slope angle

There were also evident shifts in the locations where landslides took place by comparing the occurrence of landslides in the images taken at different times. Shortly after the earthquake, the landslides were mainly distributed on terrains with mean slope angles between 30° and 50°. However, the fresh rain-induced landslides in 2010 were mainly distributed at mean slope angles between 20° and 40° (Figure 18), which were less steep. It is ascertained that a higher mean slope angle represents a steeper topography where landslides occur (Bhandary et al., 2013). Steep slopes are a typical characteristic of earthquake-induced landslides. According to Lin et al. (2006) and Xu et al. (2011), the earthquake-induced landslides on steep terrains could be attributed to topographic amplification of ground motions and reduced external loads required to trigger sliding of materials on steep slopes.

In the images taken after the rainstorm in 2010, around 10% of the fresh landslides were recognized at steep slopes between 50° and 60°. This was mainly contributed to the failure of cut slopes distributed on

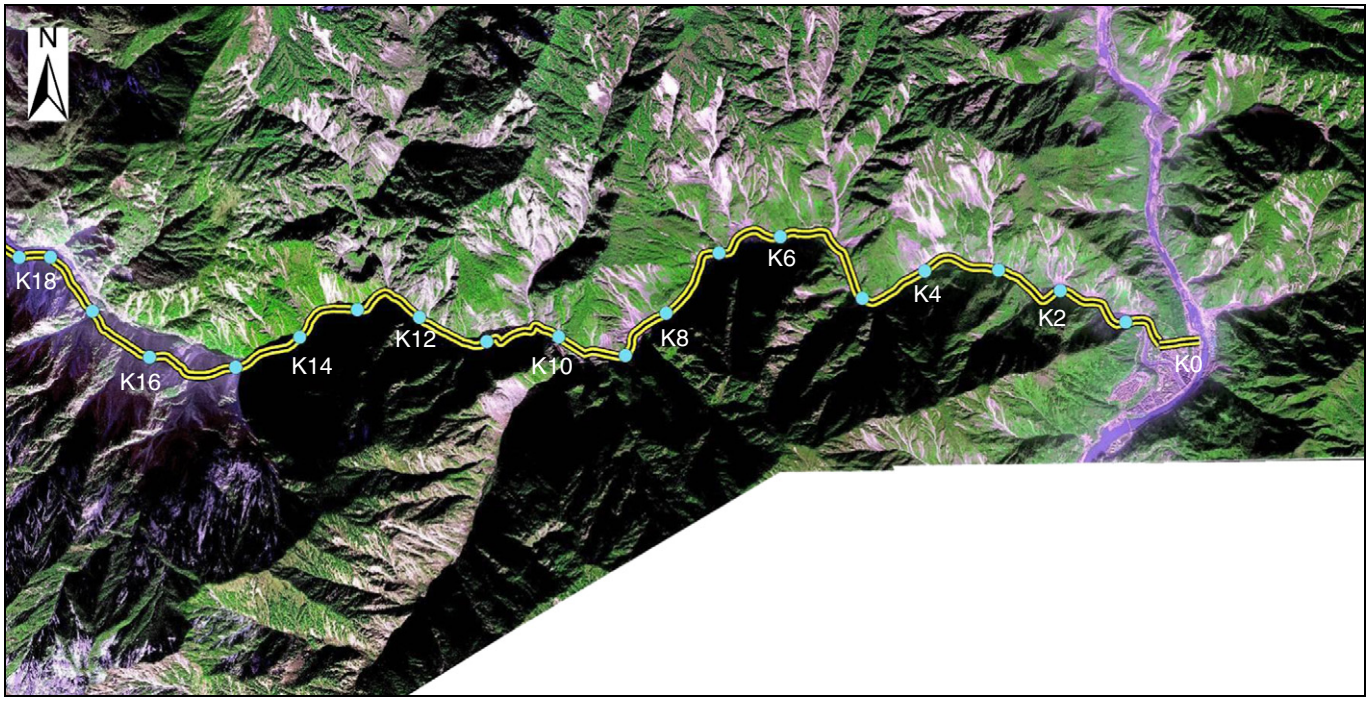

Fig. 10. Satellite image taken on 18 December 2010 showing numerous rain-induced landslides distributing along the highway.

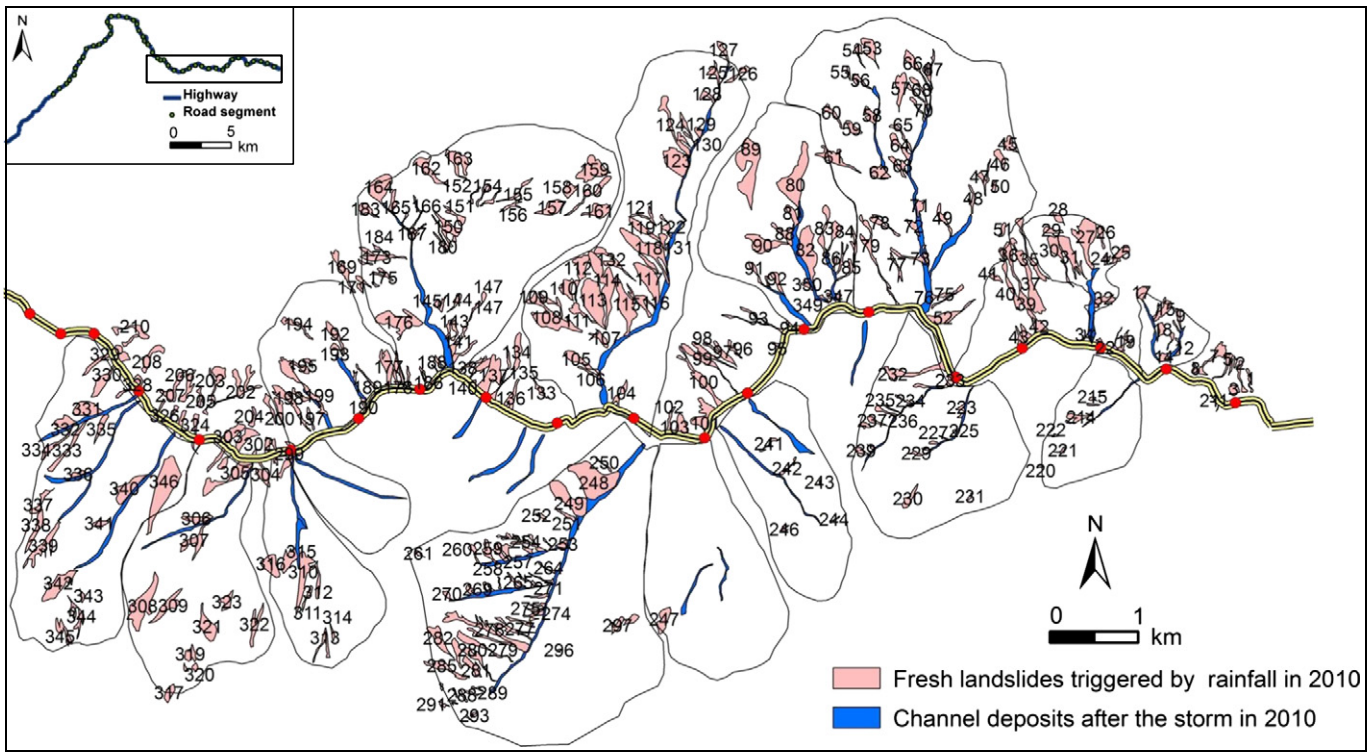

Fig. 11. Inventory of rain-induced landslides along the highway.

both sides of the road. Due to the reconstruction of the highway, slope cutting increased the slope gradients and caused stress relief in the slopes, which may aggravate slope movements during the wet season.

5.4. Variation in landslide elevation

The relationships between the landslide area and elevation are shown in Fig. 19a and b. The earthquake-induced landslides were mainly concentrated at elevations of 1500–2500 m (Figure 19a): 43% of the landslide area was recognized at elevations of 1500–2000 m and 44% at elevations of 2000–3000 m. In 2010, 29% of the rain-induced fresh landslide area was recognized at elevations of 1500–2000 and 59% at elevations of 2000–3000 m (Figure 18b). The fresh rain-induced landslides in 2010 had occurred at very high elevations where the terrain is steep. The high elevation zone also possibly experienced larger rainfall precipitation (Figure 4), which made the landslide debris there easier to be reactivated during the rainy season. Note that in this paper the landslide locations are reported as the scar locations; thus, the elevations of landslides are likely biased toward higher values.

The internal relief of a landslide is defined as the elevation difference between the scarp of the landslide and the gully mouth. It implies the potential sliding velocity and energy of its runoff debris. Most of the earthquake- and rain-induced landslides in the study area were found in zones with high internal relief values (Figure 19c and d). A total of 70% of the earthquake-induced landslides were located in areas with internal relief between 400 m and 1200 m, while only 59% of the rain-induced landslides were identified in the same range of internal relief. In a higher range of 1200–1600 m, a larger percentage of rain-induced landslides (25%) than earthquake-induced landslides (13%) were observed (Figure 19d).

A comparison of the observed internal reliefs of the earthquake-induced landslides in the study area and in other regions affected by the Wenchuan earthquake was conducted. The latter data includes 71 earthquake-induced landslides in Beichuan, Anxian, Qingchuan, Pingwu, Maoxian, and Mianzhu reported in the literature (e.g. Cui et al., 2011; Xu et al., 2011). The internal relief values of 71% of the earthquake-induced landslides in these regions were between 0 and 600 m, and only those of 4% of the earthquake-induced landslides were above 1000 m. Indeed, the earthquake-induced landslides along PR303 have much higher internal relief values than the landslides in the rest of the parts of the Wenchuan earthquake zone. The steep topography and the dominant diorite and granite hard rocks in the study area are the main reasons for this (Figures 2, 3 and 7).

5.5. Influence of lithology on the occurrence of landslides

In order to evaluate the influence of lithology on landslide density and occurrence locations, the distribution of dominant rock types and

Table 3
Landslide materials identified based on Worldwide-2 images taken on 18 December 2010.

Type	Source	Number	Total area (km^2)	Volume (10^6 m^3)
Hill-slope deposit	Reactivation landslides	322	6.61	15.42
	New landslides[a]	29	0.65	1.52
	Landslides induced by the earthquake in 2008	239	13.41	31.28
Channel deposit		35	1.69	16.94
Runout material	Channelized debris flows	12	2.33	2.80
	Hill-slope debris flows	14	0.35	0.28
Total	–		–	68.24

[a] Landslides that did not develop in the scars or deposition areas of the landslides induced by the earthquake in 2008.

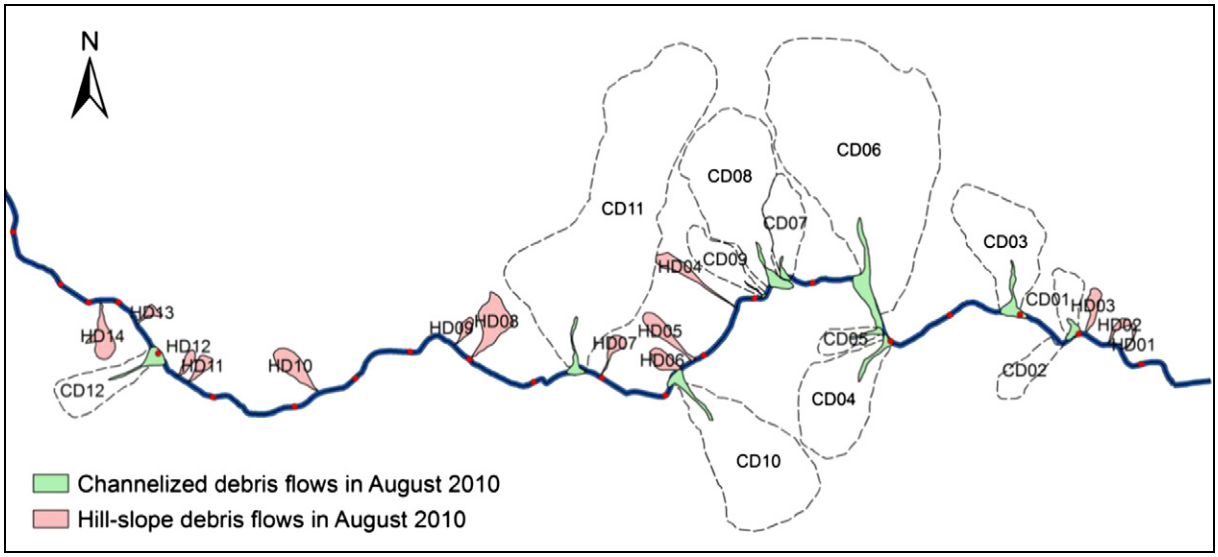

Fig. 12. Distribution of debris flows that occurred on 14 August 2010 along the highway.

the distribution of landslides in different lithology units are presented in Figs. 20 and 21. The granite zones have the largest area of landslides, which is 13.60 km^2 in 2008 and 3.97 km^2 in 2010 (Figure 20). During the earthquake, the landslides were mainly concentrated in diorite and granite zones at the mean slope angles of 30°–50° up to a maximum of 65°. The landslides in the alluvium zone were mainly distributed on terrains at the mean slope angles ranging from 10° to 30° (Figure 21a). In 2010, the fresh rain-induced landslides in diorite and granite were mainly concentrated at the mean slope angles of 20°–40°, while most of the fresh rain-induced landslides in alluvium were distributed at the mean slope angles of 15°–45° due to the increased shear strength from the presence of soil matric suction. Particularly, new rain-induced landslides in alluvium with an area ratio of 6.1% were recognized in cut slopes with the slope angles of 50°–60° (Figure 21b). The area ratio is defined as the area of landslides in each slope angle or lithology category divided by the total area of landslides.

The above observations are reasonable because the earthquake-induced landslides in diorite and granite tended to occur on steep slopes in hard rocks. The hard-rock landslide materials have high friction angles and could pose steep angles when the landslide materials ran out.

During the rainy season, most fresh landslides reactivate in the original landslide debris at high elevations and deposited on less steep terrains at lower elevations. Hence the deposit slope angles are slightly smaller than those of the earthquake-induced landslides. A relatively small number of fresh landslides reactivated in alluvium at low elevations. The relatively fine alluvium landslide materials only ran out for short distances and could form steep deposits at relatively large slope

Table 4
Basic data of debris flows along PR303 occurring in 2010.

Type	No.	Catchment area (km^2)	Volume (10^6 m^3)	Local relief[a] (m)	Max. runout distance[b] (m)
Channelized debris flow	CD01	0.37	0.160	750	250
	CD02	1.14	0.010	460	110
	CD03	1.67	0.230	720	150
	CD04	1.34	0.045	1590	200
	CD05	0.32	0.045	1060	190
	CD06	6.99	1.170	2540	593
	CD07	0.56	0.311	1140	250
	CD08	2.50	0.586	1330	600
	CD09	1.22	0.009	1420	170
	CD10	2.45	0.006	1450	80
	CD11	7.36	0.211	2480	260
	CD12	0.75	0.018	1500	210
Hill-slope debris flow	HD01	0.01	0.003	380	110
	HD02	0.03	0.004	440	90
	HD03	0.65	0.150	550	160
	HD04	0.07	0.006	940	130
	HD05	0.11	0.007	840	120
	HD06	0.11	0.003	560	110
	HD07	0.07	0.008	690	160
	HD08	0.19	0.010	980	170
	HD09	0.03	0.005	590	140
	HD10	0.09	0.004	740	100
	HD11	0.03	0.004	440	150
	HD12	0.02	0.005	380	110
	HD13	0.02	0.010	340	80
	HD14	0.11	0.062	800	250
Total	–	28.22	3.082	–	–

[a] The local relief is defined as the vertical difference in elevation between the highest and lowest points of the catchment.
[b] The runout distance is defined as the distance from the fan apex to the lowest point of the debris deposit.

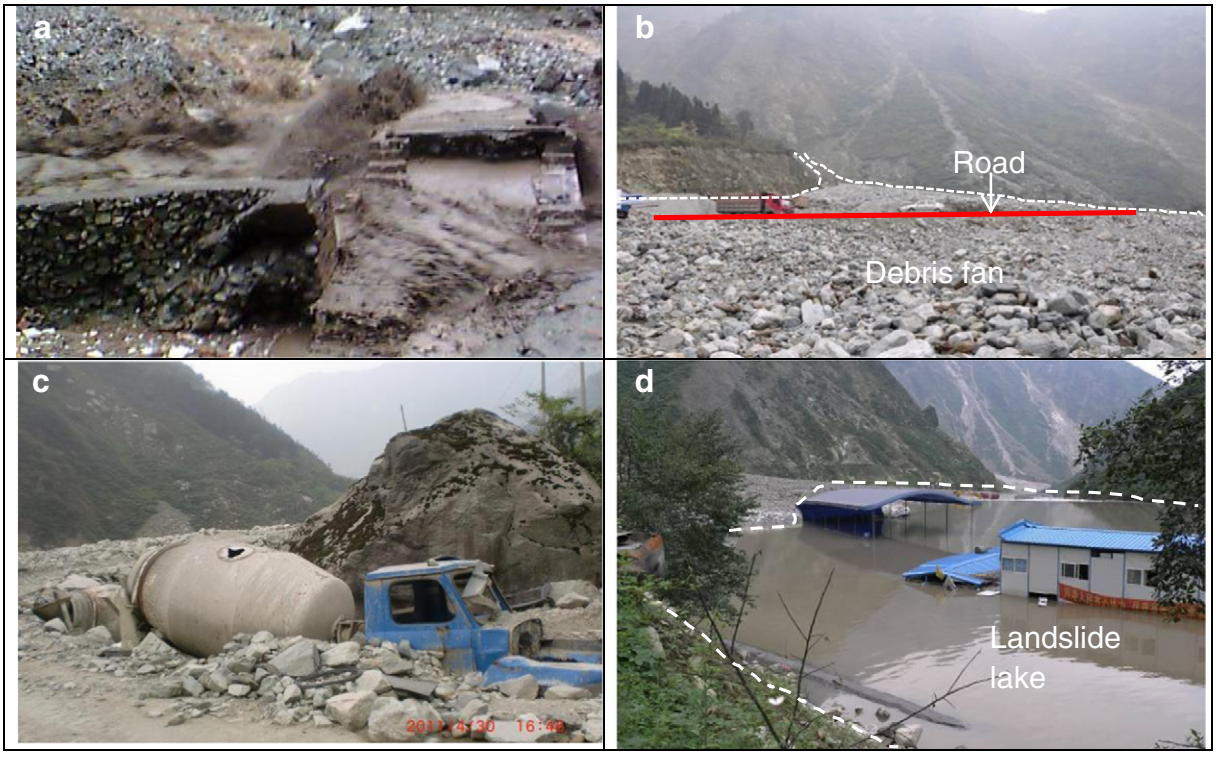

Fig. 13. Photographs taken shortly after the rainstorm: (a) occurrence of debris flow; (b) buried road under reconstruction; (c) fatalities; and (d) landslide lake.

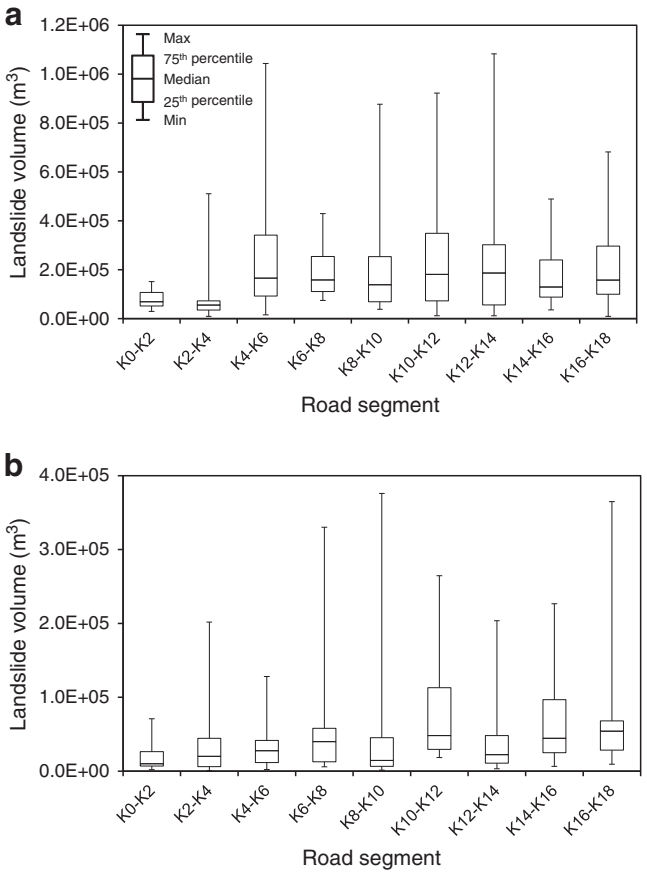

Fig. 14. Variation of volume of landslides along the highway: (a) shortly after the earthquake in 2008 and (b) shortly after the rainstorm in 2010.

angles due to the increased shear strength from the presence of soil matric suction (e.g. Fredlund et al., 1978; Zhao and Zhang, 2014).

6. Conclusions

In order to understand the influence of the Wenchuan earthquake on subsequent rain-induced landslides, landslide mapping was conducted through the interpretation of satellite images and annual field investigations along PR303 near the epicenter. Observed landslide characteristics are described and the geological and hydrological factors contributing to the initiation of landslides are presented. Several conclusions can be drawn:

(1) Shortly after the Wenchuan earthquake, 305 hill-slope deposits and 28 channel deposits were identified in the 85 km^2 study area. The total volume of the hill-slope deposits and channel deposits were 54.3 million m^3 and 12.39 million m^3, respectively. The August 2010 storm triggered a total of 351 fresh rain-induced landslides with a total volume of 16.94 million m^3. In the storm event, some of the hill-slope deposits evolved into channel deposits and the materials in the channels gradually moved forward to the gully mouth. Thus the volume of the hill-slope loose deposits decreased while the volume of the channel deposits increased.

(2) Image analysis shows that the area of earthquake-induced landslides in 2008 was 24.02 km^2 and the area of all types of landslides dropped to 20.67 km^2 in 2010. During the storm in 2010, a single debris deposit could develop into several elongated debris flows, which explains the increase of the landslide number and the decrease of the landslide area in 2010.

(3) The earthquake-induced landslides were mainly distributed at slope angles of 30°–50°. The fresh rain-induced landslides in 2010 were mainly distributed at slightly smaller slope angles between 20° and 40°. The earthquake-induced landslides were steeper, which can probably be attributed to topographic

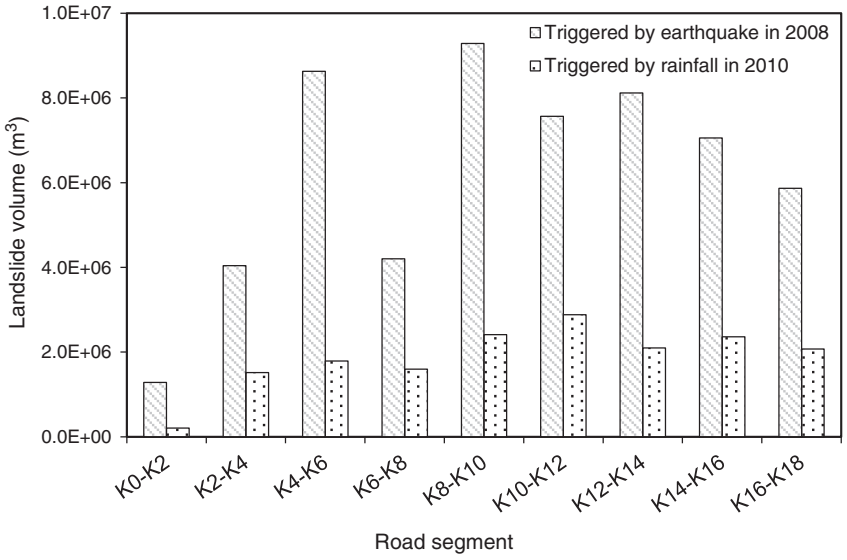

Fig. 15. Comparison of total volumes of landslides triggered by the earthquake in 2008 and the rainstorm in 2010.

amplification of ground motions and lower external loads required to trigger instability of materials on steeper slopes. In addition, the earthquake-induced landslides occurring under dry condition could pose steeper slope angles than the rain-induced landslides did.

(4) Most of the fresh rain-induced landslides in 2010 tended to occur at high elevations because the landslide scars and landslide debris in the steep area at high elevations were easier to be reactivated in the rainy season.

(5) The areas of earthquake-induced and rain-induced landslides in the granite and diorite zones are much larger than that in the alluvium zone. The earthquake-induced landslides in the granite and diorite zones are also steeper than those in the alluvium zone.

Acknowledgments

The authors gratefully acknowledge the financial support from the Sichuan Provincial Department of Transportation and Communications and the Research Grants Council of the Hong Kong SAR (No. 622210). The first author would also like to thank the University of Vienna for being the host of her exchange program during April and July 2012.

References

Bhandary, N.B., Yatabe, R., Dahal, R.K., Hasegawa, S., Inagaki, H., 2013. Areal distribution of large-scale landslides along highway corridors in central Nepal. Georisk 7, 1–20.

Chang, D.S., Zhang, L.M., Xu, Y., Huang, R.Q., 2011. Field testing of erodibility of two landslide dams triggered by the 12 May Wenchuan earthquake. Landslides 8 (3), 321–332.

Chen, H.X., Zhang, L.M., Chang, D.S., Zhang, S., 2012. Mechanisms and runout characteristics of the rainfall-triggered debris flow in Xiaojiagou in Sichuan Province, China. Nat. Hazards 62, 1037–1057.

Chen, H.X., Zhang, L.M., Zhang, S., Xiang, B., Wang, X.F., 2013. Hybrid simulation of the initiation and runout characteristics of a catastrophic debris flow. J. Mt. Sci. 10 (2), 219–232.

Cruden, D.M., Varnes, D.J., 1996. Landslide types and processes. In: Turner, A.K., Shuster, R. L. (Eds.), Landslides: Investigation and Mitigation. Transportation Research Board, Special Report 247. National Research Council, USA, pp. 36–75.

Cui, P., He, S.M., Yao, L.K., Wang, Z.Y., Chen, X.Q., 2011. The Risk Control of Landslides Induced by the Wenchuan Earthquake. Science Press, Beijing (In Chinese).

Fredlund, D.G., Morgenstern, N.R., Widger, R.A., 1978. The shear strength of unsaturated soils. Can. Geotech. J. 15, 313–321.

Glade, T., Stark, P., Dikau, R., 2005. Determination of potential landslide shear plane depth using seismic refraction — a case study in Rheinhessen, Germany. Bull. Eng. Geol. Environ. 64 (2), 151–158.

Godt, J.W., Coe, J.A., 2007. Alpine debris flow triggered by a 28 July 1999 thunderstorm in the central Front Range, Colorado. Geomorphology 84, 80–97.

Gorum, T., Fan, X.M., van Westen, C.J., Huang, R.Q., Xu, Q., Tang, C., Wang, G.H., 2011. Distribution pattern of earthquake-induced landslides triggered by the 12 May 2008 Wenchuan earthquake. Geomorphology 133, 152–167.

Harp, E.L., Jibson, R.W., 1996. Landslides triggered by the 1994 Northridge, California earthquake. Bull. Seismol. Soc. Am. 86, 319–332.

Hasi, B., Ishii, Y., Maruyama, K., 2010. Controls on distribution and scale of earthquake-induced landslides caused by the Iwate–Miyagi Inland earthquake in 2008, Japan. European Geosciences Union (EGU) General Assembly 2010, Vienna, Austria, p. 3827.

Jibson, R.W., Keefer, D.K., 1989. Statistical analysis of factors affecting landslide distribution in the New Madrid seismic zone, Tennessee and Kentucky. Eng. Geol. 27, 509–542.

Jibson, R.W., Harp, E.L., Schulz, W., Keefer, D.K., 2004. Landslides triggered by the 2002 Denali Fault, Alaska, earthquake and the inferred nature of the strong shaking. Earthquake Spectra 20, 669–691.

Keefer, D.K., 1984. Landslides caused by earthquakes. Bull. Geol. Soc. Am. 95, 406–421.

Khazai, B., Sitar, N., 2004. Evaluation of factors controlling earthquake-induced landslides caused by Chi-Chi earthquake and comparison with the Northridge and Loma Prieta events. Eng. Geol. 71, 79–95.

Li, X.J., Zhou, Z.H., Yu, H.Y., 2008. Strong motion observations and recordings from the great Wenchuan Earthquake. Earthq. Eng. Eng. Vib. 7, 235–246.

Lin, C.W., Wang, K.L., Chen, T.C., 2000. Characteristics of the slope failure caused by the Chi-Chi earthquake. International Workshop on Annual Commemoration of Chi-Chi Earthquake, September 18–20, 2000, Taipei. vol. 3, pp. 199–209.

Lin, C.W., Liu, S.H., Lee, S.Y., Liu, C.C., 2006. Impacts of the Chi-Chi earthquake on subsequent rainfall-induced landslides in central Taiwan. Eng. Geol. 86, 87–101.

Mantovani, F., Soeters, R., Van Westen, C.J., 1996. Remote sensing techniques for landslide studies and hazard zonation in Europe. Geomorphology 15, 213–225.

Martin, Y., Rood, K., Schwab, J.W., Church, M., 2002. Sediment transfer by shallow landsliding in the Queen Charlotte Islands, British Columbia. Can. J. Earth Sci. 39, 189–205.

Qi, S.W., Xu, Q., Lan, H.X., Zhang, B., Liu, J.Y., 2010. Spatial distribution analysis of landslides triggered by 2008.5.12 Wenchuan earthquake, China. Eng. Geol. 116, 95–108.

Sato, H.P., Hsegawa, H., Fujiwara, S., Tobita, M., Koarai, M., Une, H., Iwahashi, J., 2007. Interpretation of landslide distribution triggered by the 2005 Northern Pakistan earthquake using SPOT5 imagery. Landslides 4, 113–122.

Sichuan Highway Department, 2011. Feasibility of the Reconstruction of Province Road 303 from Yingxiu to Wolong. Sichuan Highway Department, Chengdu, Sichuan (In Chinese).

Tang, C., Zhu, J., Qi, X., Ding, J., 2011. Landslides induced by the Wenchuan earthquake and the subsequent strong rainfall event: a case study in the Beichuan area of China. Eng. Geol. 122, 22–33.

Varnes, D.J., 1958. Landslide types and processes. In: Eckel, E.B. (Ed.), Landslides and Engineering Practice: Highway Research Board Special Report 29, pp. 20–47.

Xu, Q., Zhang, S., Li, W.L., 2011. Spatial distribution of large-scale landslides induced by the 5.12 Wenchuan earthquake. J. Mt. Sci. 8, 246–260.

Yin, Y.P., 2008. Researches on the geo-hazards triggered by Wenchuan earthquake, Sichuan. J. Eng. Geol. 16 (4), 433–444 (In Chinese).

Yin, Y.P., Wang, F.W., Sun, P., 2009. Landslide hazards triggered by the 2008 Wenchuan earthquake, Sichuan, China. Landslides 6, 139–151.

Zhang, L.L., Fredlund, D.G., Zhang, L.M., Tang, W.H., 2004. Numerical study of soil conditions under which matric suction can be maintained. Can. Geotech. J. 41 (4), 569–582.

Zhang, L.L., Zhang, J., Zhang, L.M., Tang, W.H., 2011. Stability analysis of rainfall-induced slope failures: a review. Proc. Inst. Civ. Eng. Geotech. Eng. 164 (5), 299–316.

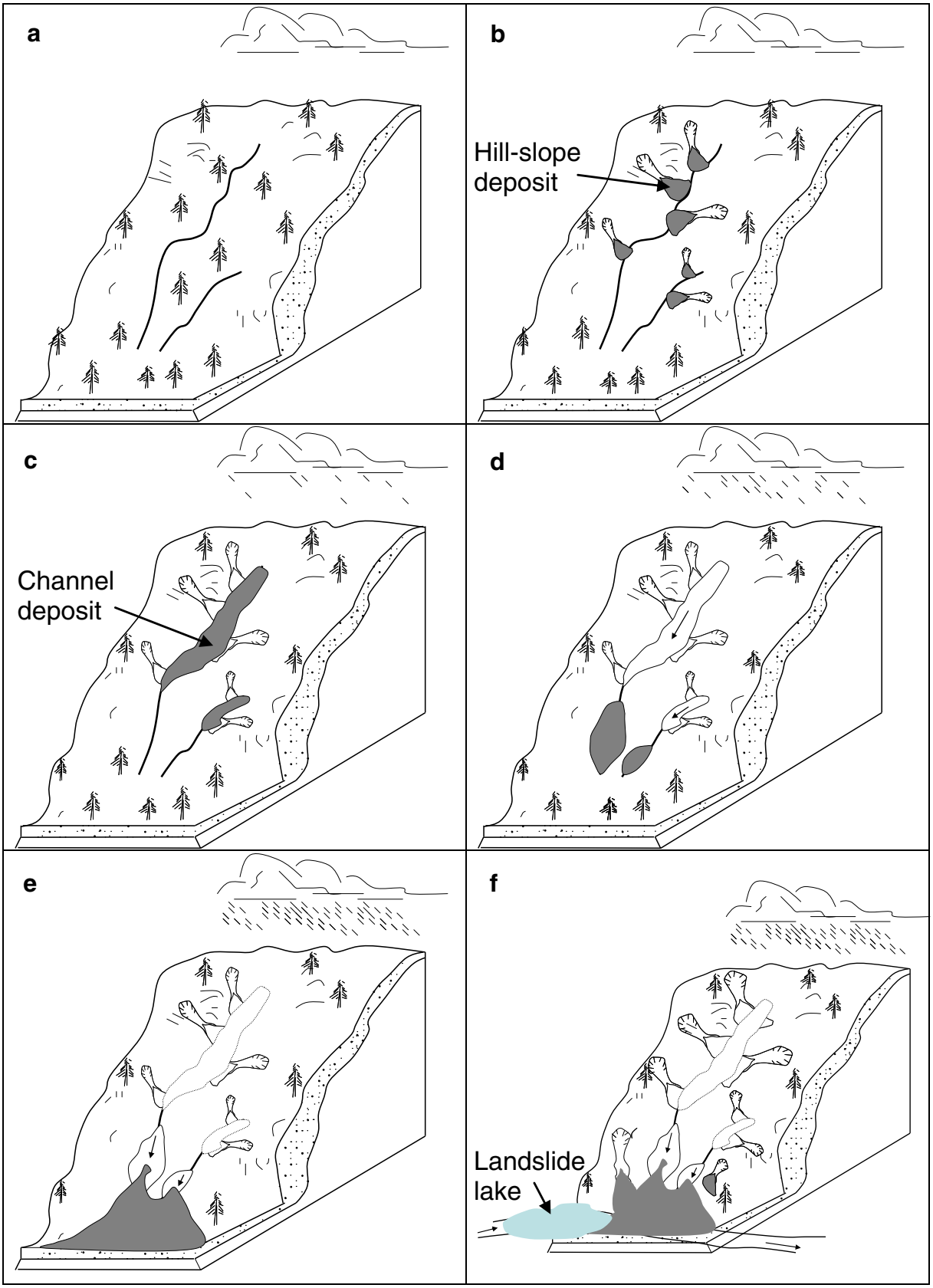

Fig. 16. Evolution of loose materials into debris flows: (a) initial state; (b) loose materials retained on steep hill slopes; (c) evolving into channel deposits; (d) moving toward the gully mouth; (e) debris flow; and (f) landslide lake.

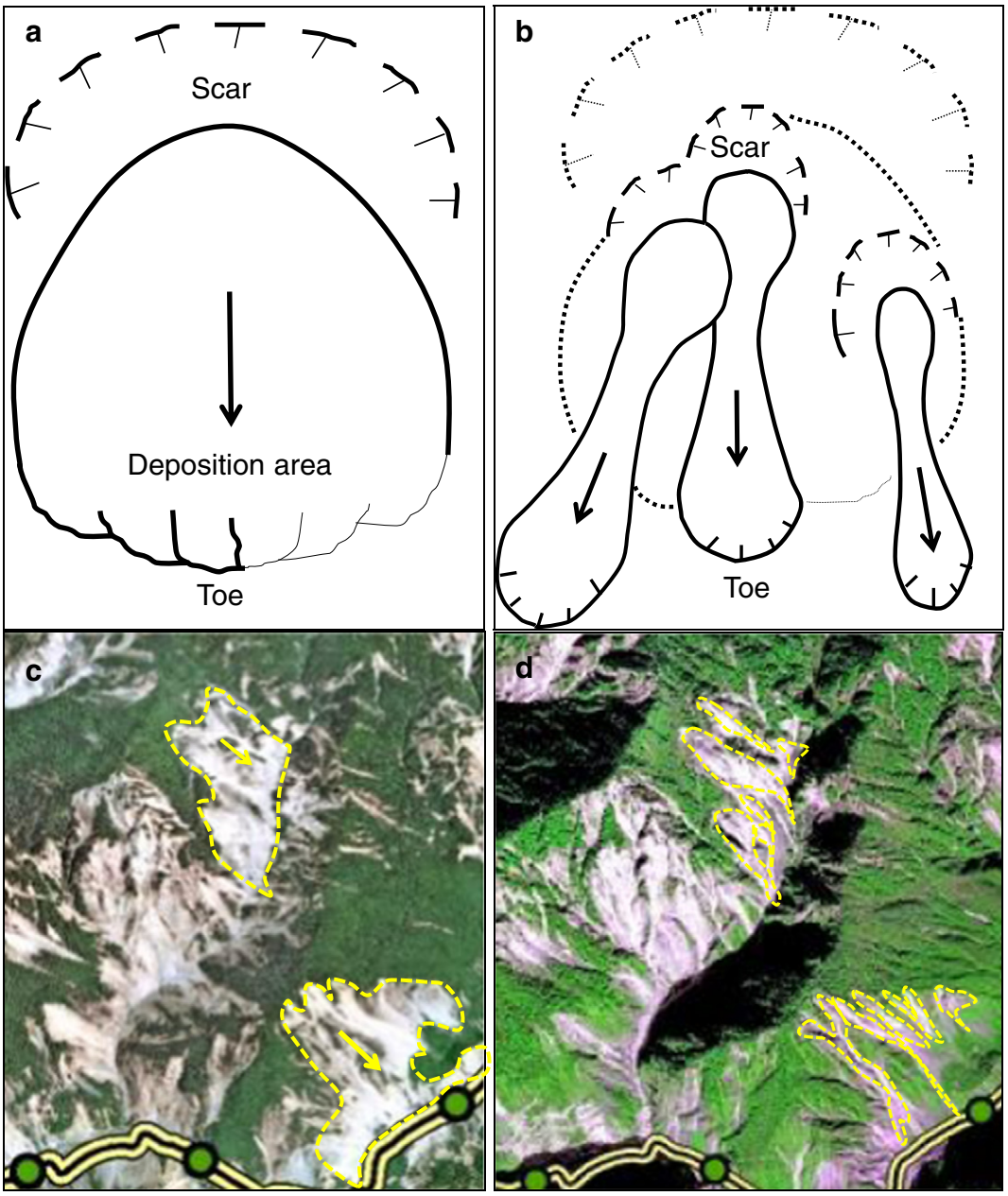

Fig. 17. Change in the type of landslides: (a) debris slide triggered by the earthquake in 2008; (b) debris flow triggered by rainfall in 2010; (c) real case in 2008; and (d) real case in 2010.

Zhang, S., Zhang, L.M., Peng, M., Zhang, L.L., Zhao, H.F., Chen, H.X., 2012. Assessment of risks of loose landslide deposits formed by the 2008 Wenchuan earthquake. Nat. Hazards Earth Syst. Sci. 12 (5), 1381–1392.
Zhang, S., Zhang, L.M., Chen, H.X., Yuan, Q., Pan, H., 2013. Changes in runout distances of debris flows over time in the Wenchuan earthquake zone. J. Mt. Sci. 10, 281–292.
Zhao, H.F., Zhang, L.M., 2014. Instability of saturated and unsaturated coarse granular soils. J. Geotech. Geoenviron. 140 (1), 25–35.
Zhao, H.F., Zhang, L.M., Fredlund, D.G., 2013. Bimodal shear strength behavior of unsaturated coarse-grained soils. J. Geotech. Geoenviron. 139 (12), 2070–2081.

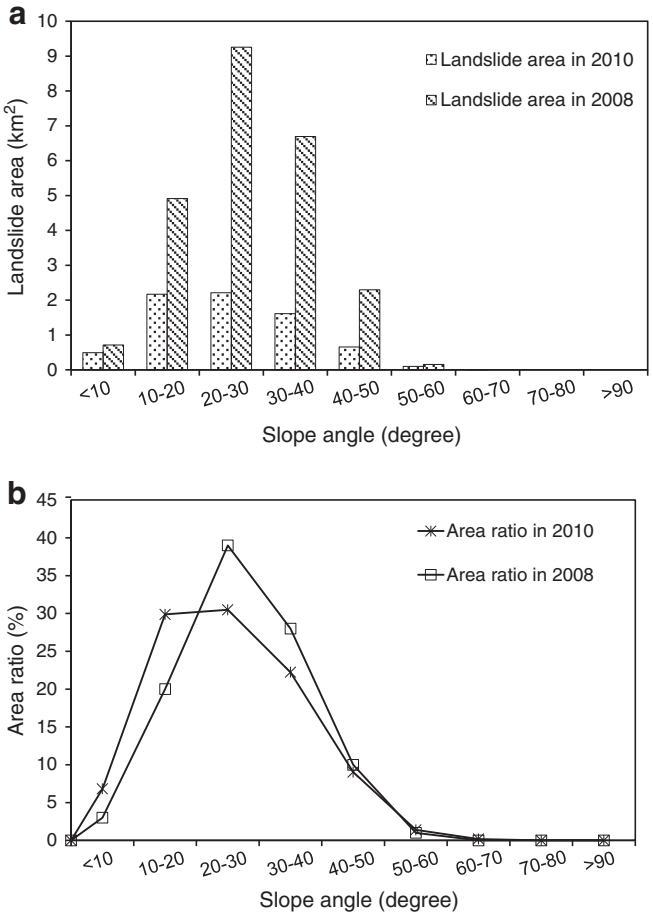

Fig. 18. Distribution of landslides of different slope angles: (a) landslide area; (b) area ratio.

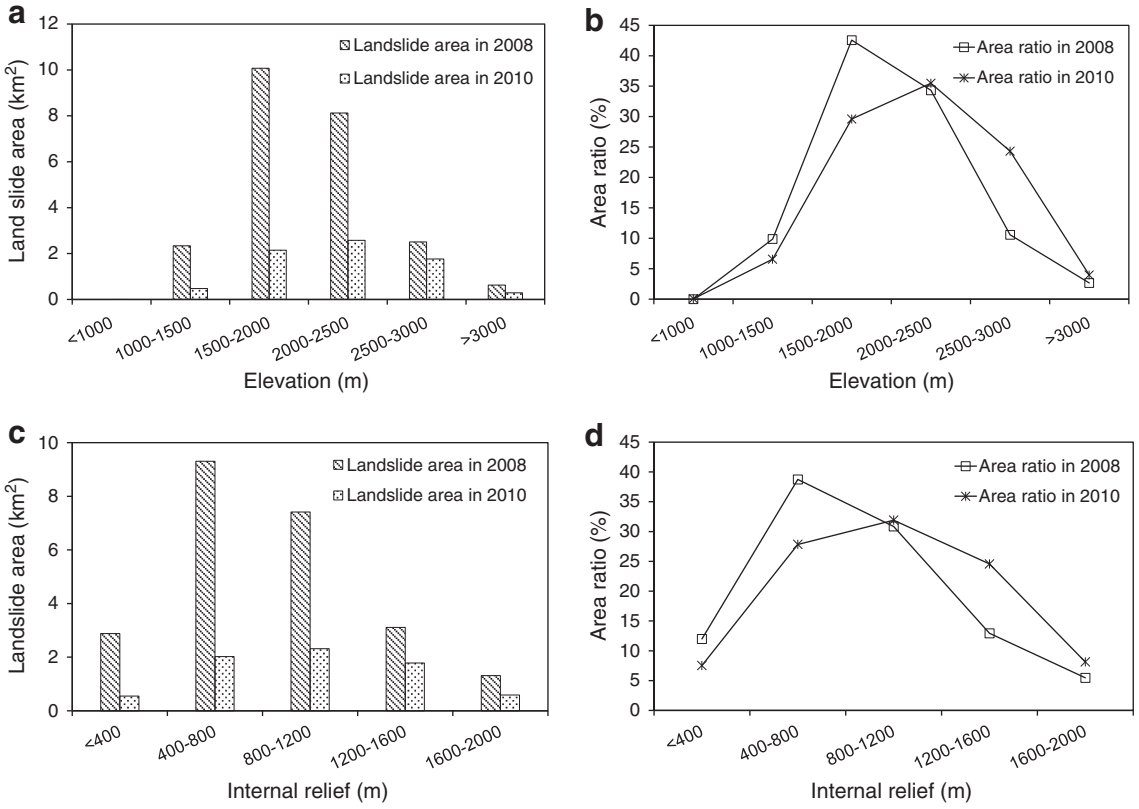

Fig. 19. Distributions of landslide area and area ratio: (a) and (b) with elevation; (c) and (d) with internal relief.

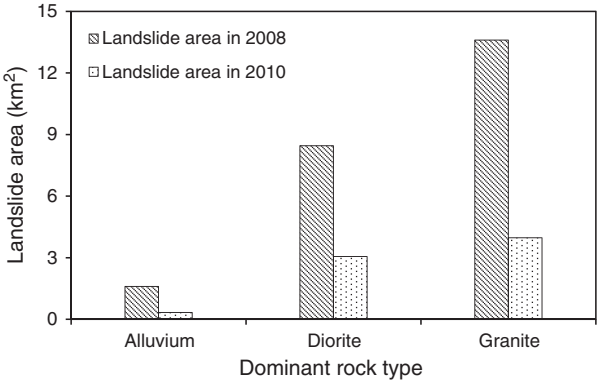

Fig. 20. Distribution of landslides in areas of different dominant rock types.

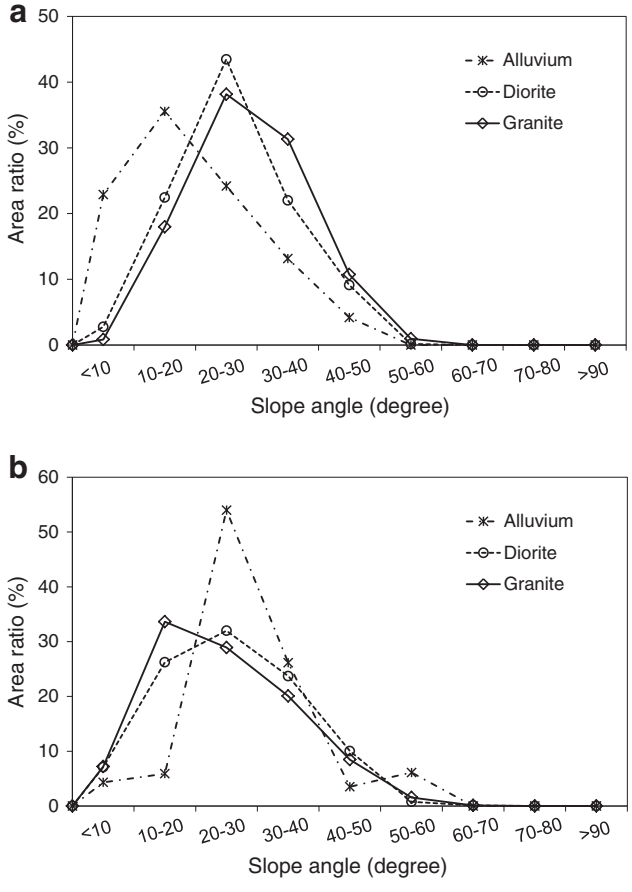

Fig. 21. Landslides in different lithology units: (a) landslides in 2008 and (b) landslides in 2010.